Cell Reports, Volume *42*

Supplemental information

Neprilysin-dependent neuropeptide Y cleavage in the liver promotes fibrosis by blocking NPY-receptor 1

Cristina Ortiz, Sabine Klein, Winfried H. Reul, Fernando Magdaleno, Stefanie Gröschl, Peter Dietrich, Robert Schierwagen, Frank E. Uschner, Sandra Torres, Christoph Hieber, Caroline Meier, Nico Kraus, Olaf Tyc, Maximilian Brol, Stefan Zeuzem, Christoph Welsch, Marco Poglitsch, Claus Hellerbrand, Mercedes Alfonso-Prieto, Fabio Mira, Ulrich auf dem Keller, Anja Tetzner, Andrew Moore, Thomas Walther, and Jonel Trebicka

SUPPLEMENTARY RESULTS

Supplementary Table 1. Statistics of the top best cluster for each of the HADDOCK docking runs performed

	NPY C-terminal fragments	
	Y_1R-NPY(21-36)	**Y_1R-NPY(31-36)**
Cluster rank	1	1
Cluster population	**112**	**197**
HADDOCK score* (a.u.)	-141.0 ± 13.6	-123.8 ± 8.2
RMSD from the overall lowest energy structure (Å)	0.7 ± 0.5	0.7 ± 0.4
Intermolecular van der Waals energy (E_{vdw})(kcal mol^{-1})	-59.7 ± 5.4	-52.2 ± 3.6
Intermolecular electrostatic energy (E_{elec})(kcal mol^{-1})	-219.0 ± 56.0	-172.4 ± 30.8
Desolvation energy (E_{desol})(kcal mol^{-1})	-6.0 ± 7.5	-15.4 ± 5.9
Restraints violation energy (E_{AIR})(kcal mol^{-1})	791.4 ± 96.57	682.2 ± 74.21
Buried surface area ($Å^2$)	1799.1 ± 55.6	1459.9 ± 10.1
Z-score	-1.3	0.0
Distance between Gln120-Tyr36 (Å)	9.4	11.88

*The HADDOCK score is defined as 1.0 E_{vdw} + 0.2 E_{elec} + 1.0 E_{desol} + 0.1 E_{AIR}.

Supplementary Table 2. List of commercially available antibodies used

Name	**CAT #**	**Company**
Col1a1	1310-01	Southern Biotech
αSMA	ab5694	Abcam plc, Cambridge
GAPDH	sc-25778	Santa Cruz Biotechnology
SMAD2	D43B4	Cell Signaling
SMAD3	C67H9	Cell Signaling
pSMAD2	138D4	Cell Signaling
pSMAD3	C25A9	Cell Signaling
RhoA	sc-418	Santa Cruz Biotechnology
ROCK2	sc-5561	Santa Cruz Biotechnology
PCNA	sc-56	Santa Cruz Biotechnology
p-Moesin	sc-12895	Santa Cruz Biotechnology

NPY	11976S	Cell Signalling

Supplementary Table 3. Primer sequences

Gene name	Assay ID	Specie
acta2	Mm00725412_s1	*Mus musculus*
col1a1	Mm00801666_g1	*Mus musculus*
edn-1	Mm00438656_m1	*Mus musculus*
edn-2	Mm00432983_m1	*Mus musculus*
ednra	Mm01243722_m1	*Mus musculus*
ednrb	Mm00432989_m1	*Mus musculus*
npy	Mm01410146_m1	*Mus musculus*
Nep (MME)	Mm00485028_m1	*Mus musculus*
npyr1	Mm00650798-g1	*Mus musculus*
npyr2	Mm01956783_s1	*Mus musculus*
npyr5	Mm02620267-s1	*Mus musculus*
tgfβ-1	Mm03024053_m1	*Mus musculus*
vegfa	Mm00437306_m1	*Mus musculus*
F4/80	Mm00802529_m1	*Mus muscullus*
Arg1	Mm00475988_m1	*Mus musculus*
Ccr2	Mm99999051_gH	*Mus musculus*
Fap	Mm01329175_m1	*Mus musculus*
Dpp4	Mm00494552_m1	*Mus musculus*
MME	Hs00153510_m1	*Homo sapiens*
Npyr1	Hs00702150_s1	*Homo sapiens*
Npyr2	Hs01921296_s1	*Homo sapiens*
Npyr5	Hs01883189_s1	*Homo sapiens*

Supplementary Table 4. Complete list of restraints used in the information-driven docking of the C-terminal fragments NPY(21-36) and NPY(31-36) to Y_1R.

1. Experimentally-based restraints
NPY(31-36)/Y_1R: Y36-Y100$^{2.64}$, Y36-W106^{ECL1}, Y36-Q120$^{3.32}$, R35-N283$^{6.55}$, R35-D287$^{6.59}$, R33-N299$^{7.32}$ *NPY(21-36)/Y_1R:* Y36-Y100$^{2.64}$, Y36-W106^{ECL1}, Y36-Q120$^{3.32}$, R35-N283$^{6.55}$, R35-D287$^{6.59}$, R33-N299$^{7.32}$, L30-I293^{ECL3}, R25-D104$^{2.67}$
2. Fpocket-based restraints

NPY(31-36) or NPY(21-36): all residues of the corresponding fragment *Y_1R:* D31, C33, C93, C94, T97, Y100, T101, D104, W106, C113, N116, P117, Q120, C121, I124, F173, Q177, P183, F184, N186, V187, K195, V197, C198, F199, D200, F202, R208, Y211, T212, C215, C216, Q219, Y220, F272, W276, C279, T280, F282, N283, T284, F286, D287, N289, H290, Q291, I292, I293, A294, T295, C296, H298, N299, F302, H306, M310
3. Center of mass restraint
NPY(31-36) or NPY(21-36): center of all Cα atoms *Y_1R:* center of all Cα atoms
4. Extracellular loop-based restraints
NPY(21-36): residues 21-32 *Y_1R:* residues 105-108 (ECL1) and residues 290-294 (ECL3)

1. The experimentally-based restraints were derived from references[25,44]. Here, the first number indicates the residue of the NPY fragment, while the second corresponds to Y_1R; for the latter, both the human Y_1R sequence numbering and the Ballesteros-Weinstein numbering for class A GPCRs are given. The experimentally-based restraints were defined as unambiguous restraints, i.e. they are enforced in all the docking structures.

2. The fpocket-based restraints involve all residues of the corresponding NPY fragment and the Y_1R residues predicted to be part of the binding cavity by fpocket [45,46] . Therefore, only the fpocket-predicted residues are explicitly listed. These computationally-based restraints were defined as ambiguous restraints, so that 50% of them are randomly deleted in each docking trial in order to minimize any possible artefact due to an incorrectly predicted binding cavity residue.

Nevertheless, we would like to note here that residues Y100, N283, D287, I293 and N299, which have been experimentally proven to interact with the C-terminal part of NPY [25], are also predicted by fpocket as part of the binding cavity, providing support to the computational prediction.

3. The center of mass restraint is an ambiguous distance restraint between the centers of the two molecules. The center of each molecule is defined as the average of all its Cα atoms [47].

4. The ECL-based restraints were chosen based on the putative positioning of the central α-helix (A14-T32) near the Y_1R extracellular loops ECL1 and ECL3[25]. In particular, the ECL-based restraints involve the residues of the NPY(21-36) fragment forming part of the central α-helix (residues 21-32) and the Y_1R residues belonging to ECL1 and ECL3 (residues 105-108 and 290-294, respectively, according to the GPCR database (www.gpcrdb.org/protein/npy1r_human/)). These ECL-based restraints were defined as unambiguous restraints, as are the fpocket-based restraints, except that the upper limit of the effective distance was increased from 2.0 Å (default value) to 5.0 Å. In this way, the central α-helix can be guided towards the extracellular loops, but without necessarily enforcing a direct interaction.

SUPPLEMENTARY FIGURES

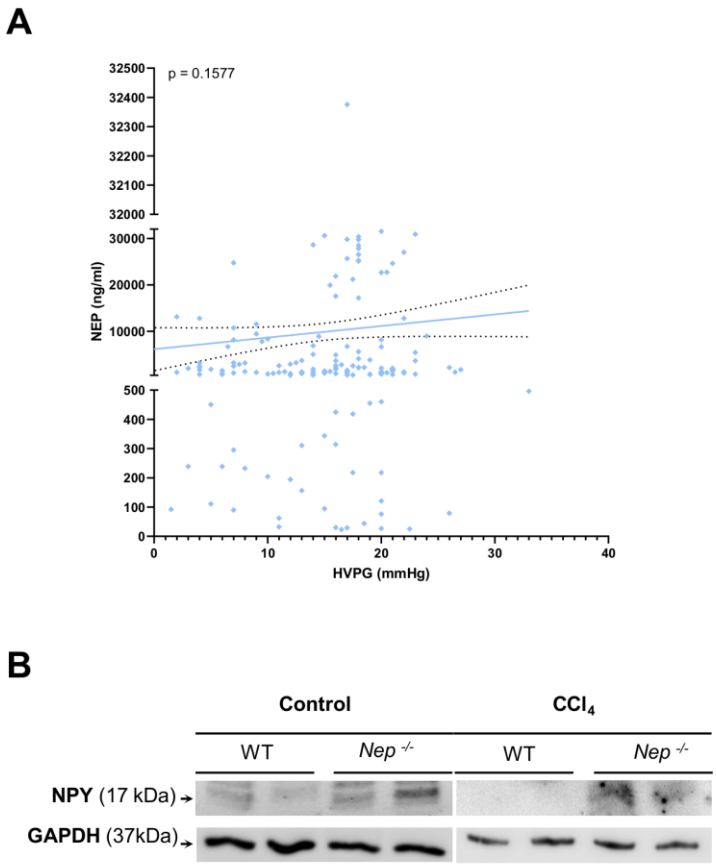

Supplementary Figure 1. Correlation of NEP levels and portal hypertension in patients with cirrhosis. (A) A simple linear regression with 95% confidence interval was made to show the trend between NEP levels and hepatic venous pressure gradient (HVPG) in 125 cirrhosis patients. *p* value and *r*=0.1029 were calculated with non-parametric (Spearman) correlation. **(B)** Western blot analysis of NPY protein from controls vs. CCl_4-treated *Nep*$^{-/-}$ mice and WT mice. The expression of GAPDH was used as a loading control.

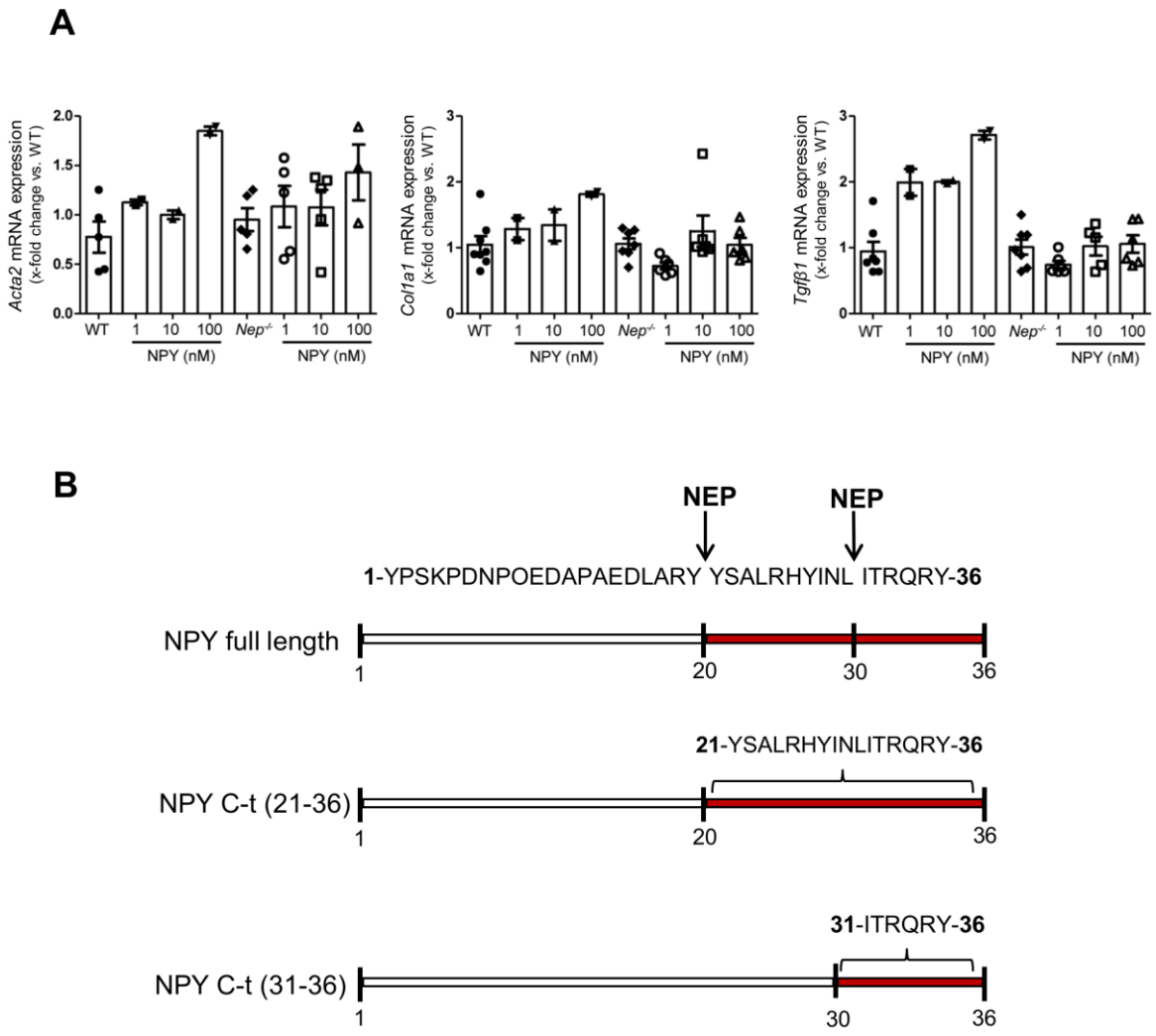

Supplementary Figure 2. Diagram of NPY and its fragments generated by NEP proteolysis. (A) qPCR analysis from *Acta2, Col1a1* and *Tgfβ1* of HSCs from WT and *Nep*$^{-/-}$ mice treated with different NPY protein concentrations (1, 10 and 100nM) to determine the right dose of recombinant NPY protein. All data were normalized to the expression of *18sRNA*. **(B)** Illustration of full length NPY amino acid sequence showing the two potential cleavage sites for NEP and the two final NPY short peptides that are generated.

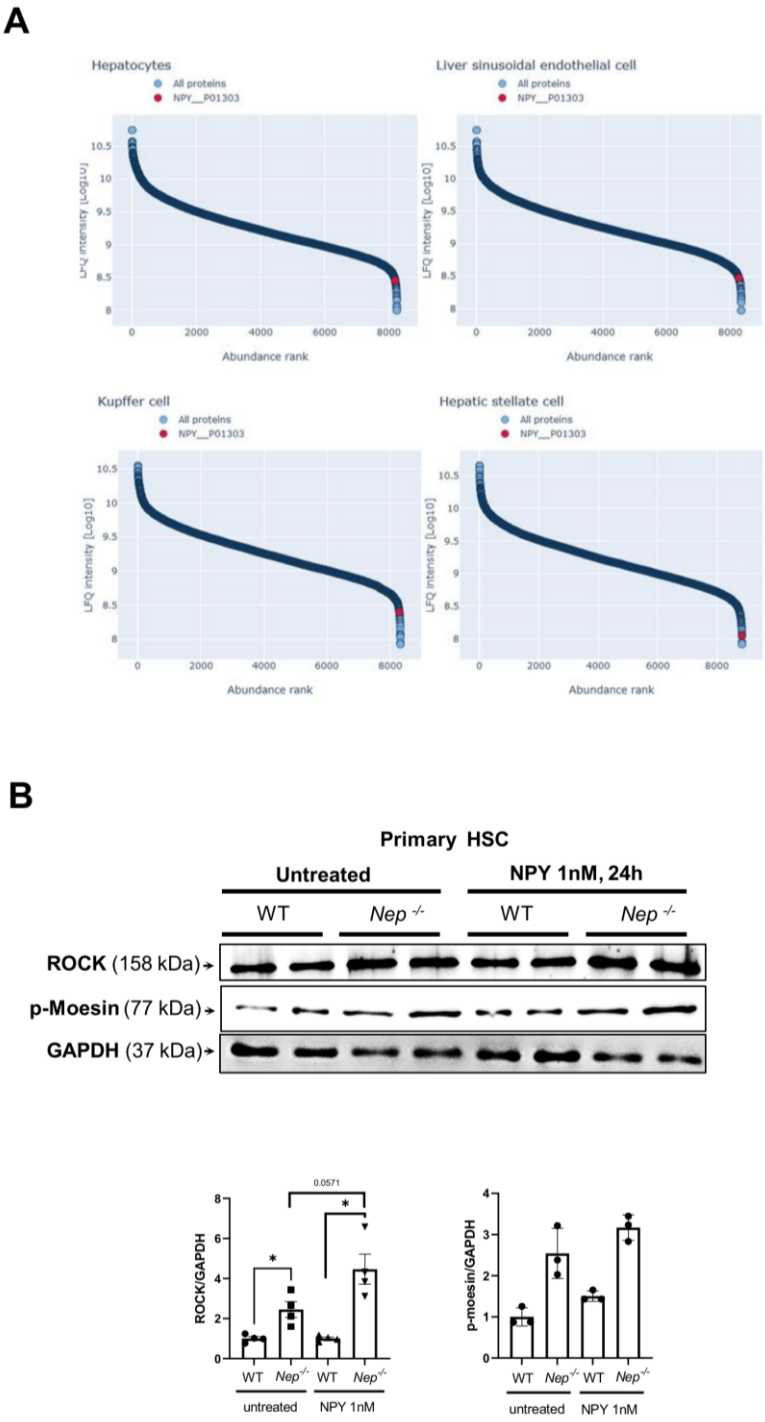

Supplementary Figure 3. NPY abundance and its effect in HSC (A) Analysis of abundance of NPY protein in the different hepatic cell types. **(B)** Western blot from primary HSC isolated from WT and *Nep*$^{-/-}$ mice treated with and without NPY 1 nM for 24 h. Results are expressed as mean ± standard error of the mean (SEM); **p*<0.05, ***p*<0.01 for NPY-treated *vs*. corresponding control HSC.

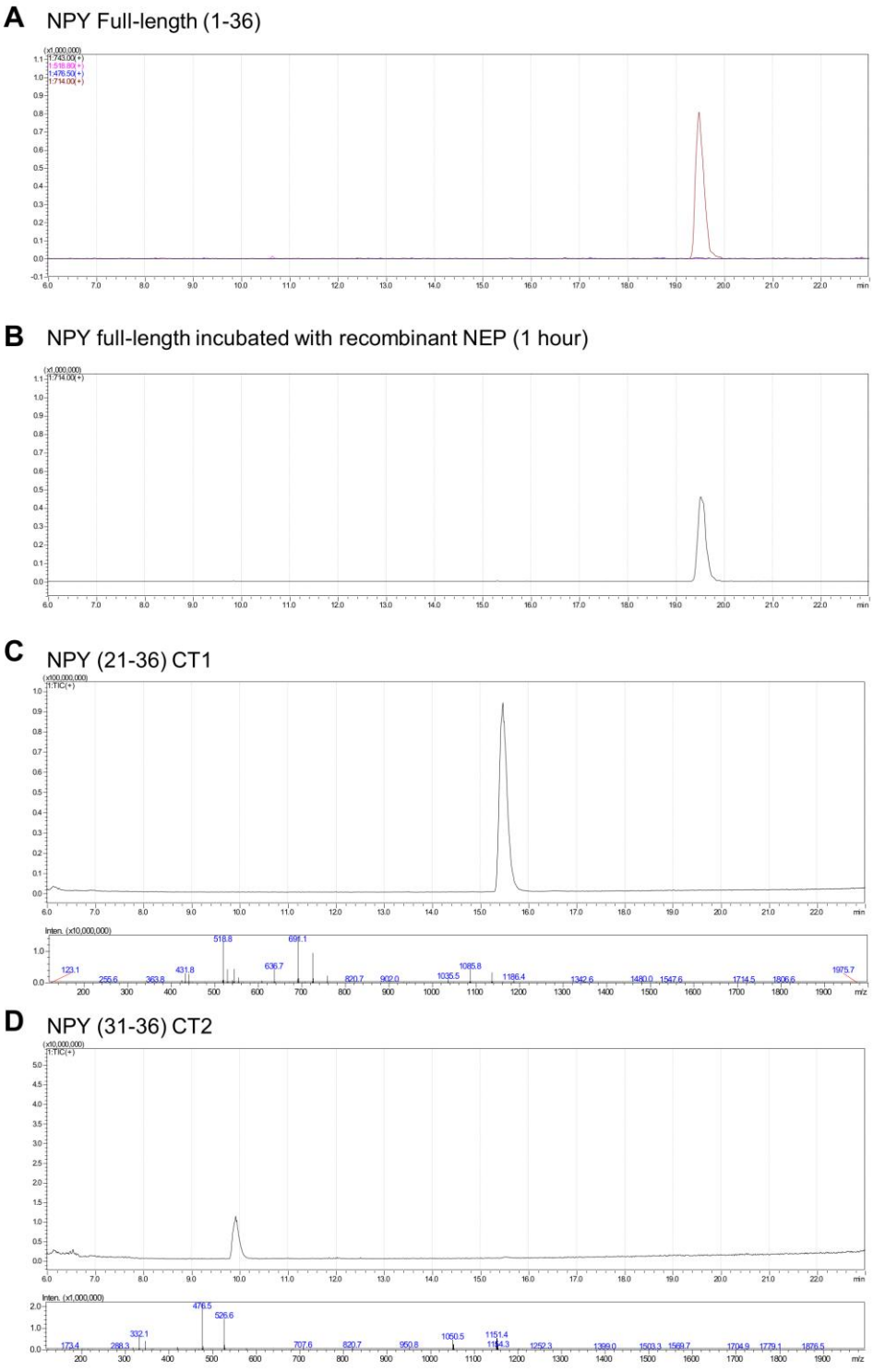

Supplementary Figure 4. Characterization of NPY, NEP cleavage of NPY and NPY C-terminal short fragments. (A-D) LCMS measurements of NPY full length showing the elution profile. Incubation of NPY together with NEP for 1 h decreased the amount of NPY protein but the expected corresponding NPY short C-terminal fragments were not present. Synthetic NPY C-terminal fragments, (21-36) and (31-36), were run independently to analyze their retention times, stability, and specific m/z peaks.

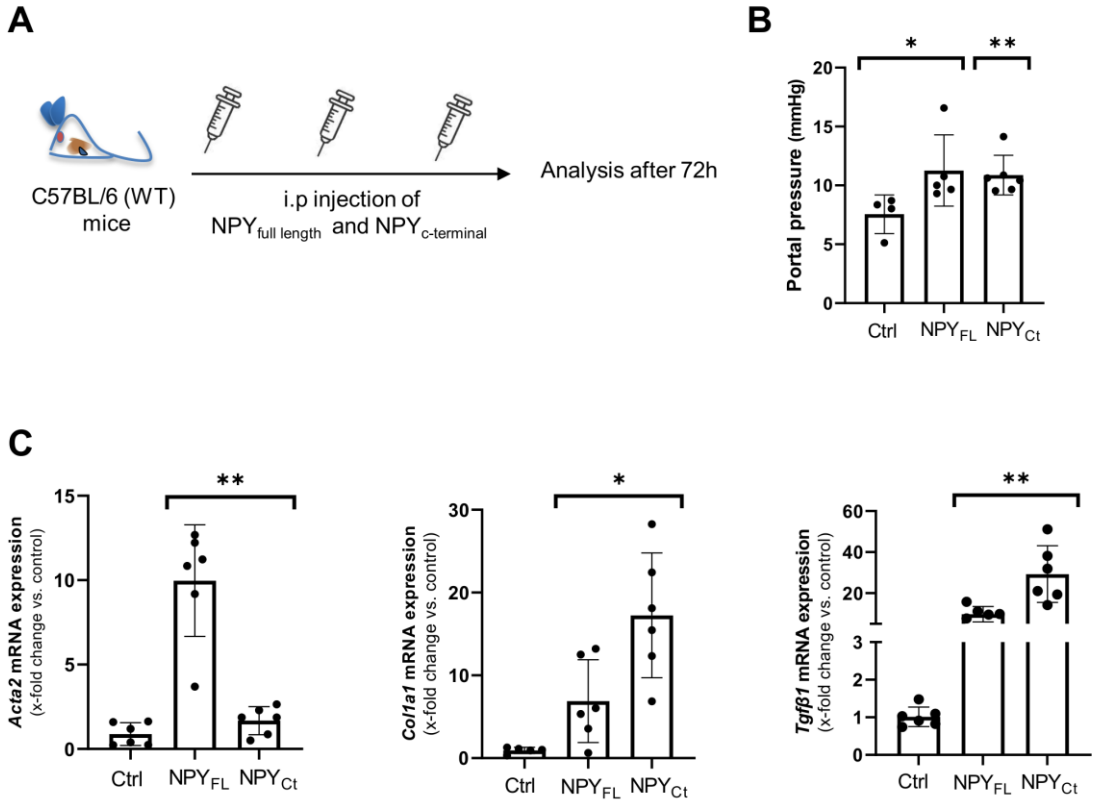

Supplementary Figure 5. ***In vivo*** **effect in mice of full length NPY and its C-terminal fragments. (A)** Schematic representation of the mice treated for 72 hours with full length NPY and NPY C-terminal cleaved fragments. **(B)** Portal pressure measurements from the three different mice groups, **(C)** Hepatic *Acta2*, *col1a1* and *Tgfβ1* mRNA expression of the different mice groups untreated and treated with full length NPY and its C-terminal fragments. All data were normalized to the expression of *18sRNA*. Results are expressed as mean ± standard error of the mean (SEM), n=6/group.; **p*<0.05, ***p*<0.01,

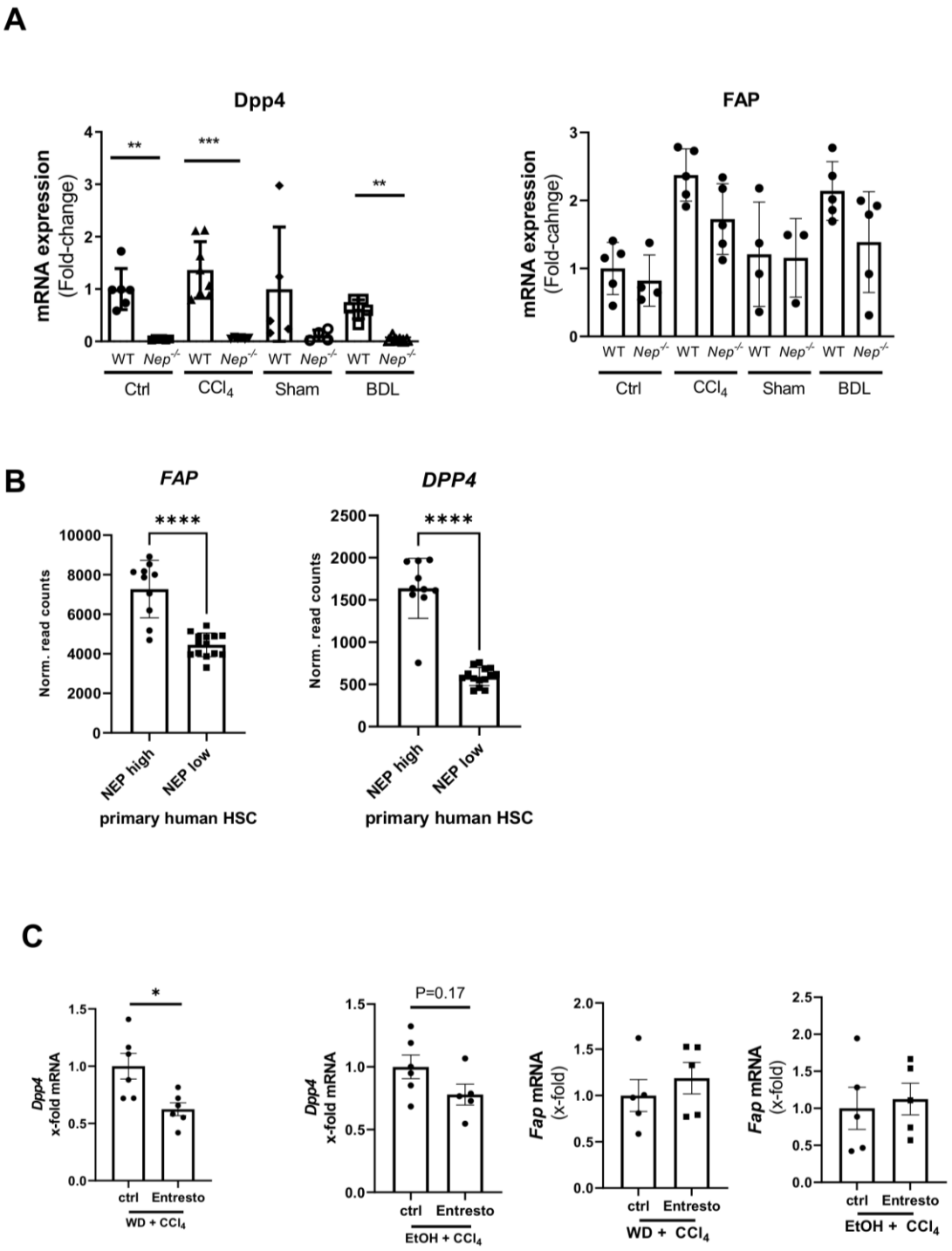

Supplementary Figure 6. Analysis of *Dpp4* and *FAP* expression. (A) *Dpp4* and *FAP* mRNA expression in WT and CCl_4- and BDL-treated *Nep*$^{-/-}$ mice. *Nep*$^{-/-}$-treated mice showed decreased expression of *Dpp4* compared to WT mice. *FAP* was slightly reduced in *Nep*$^{-/-}$ mice. n=6/group. ***p*<0.01, ****p*<0.001. **(B)** Normalized read counts of FAP and Dpp4 expression in human primary HSCs transcriptomic data. *****p*<0.0001. **(C)** mRNA expression of *Fap* and *Dpp4* in fibrotic WT mice treated with Entresto®. Mice treated with Entresto® showed no significant upregulation of *Fap* expression compared to the controls. *Dpp4* expression was significantly downregulated in mice treated with Entresto® compared to controls. All data were normalized to the expression of *18sRNA*. Results are expressed as mean ± standard error of the mean (SEM); **p*<0.05.

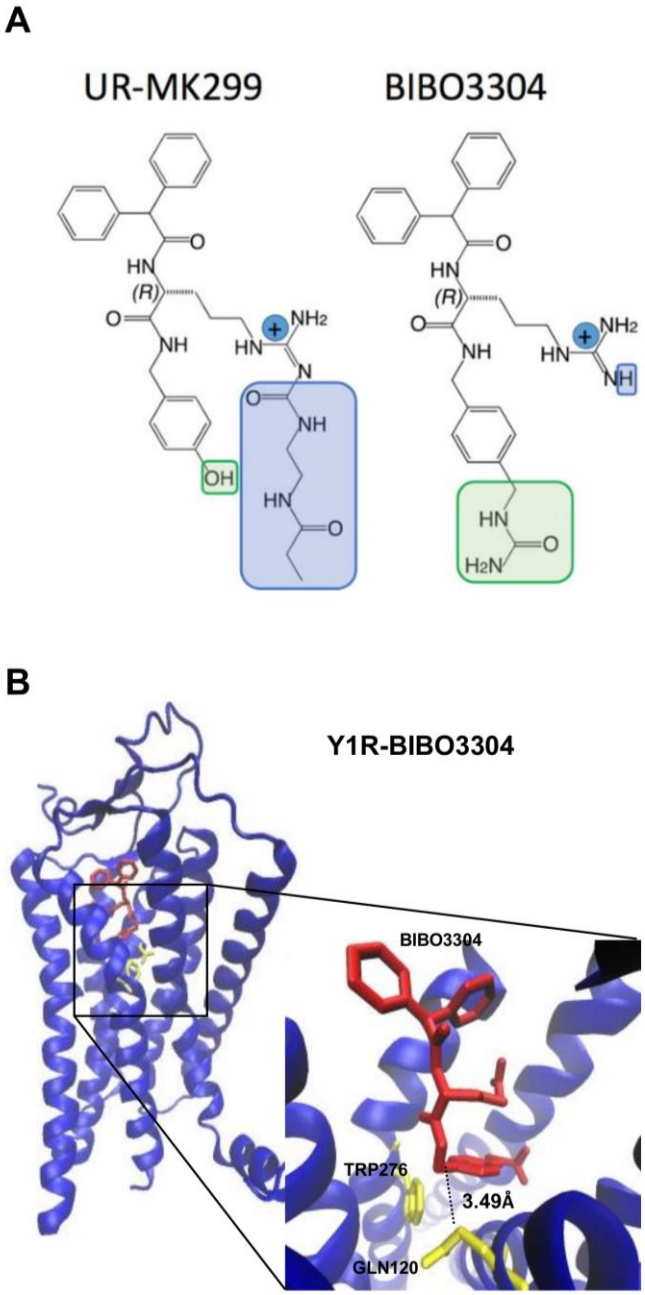

Supplementary Figure 7. Comparison of the chemical structures of the antagonists BIBO3304 and UR-MK299. (A) The chemical structure of BIBO3304 is designed to mimic the C-terminal NPY residues Arg35 and Tyr36 and shares the same scaffold with UR-MK299. Hence, the model of the Y_1R/BIBO3304 complex was built by manual modification of the experimental structure of the Y_1R/UR-MK299 complex (PDB code 5ZBQ) (1). In particular, the carbamoyl tail (in blue) was removed from the guanidinium group, and the hydroxyl group (in green) was replaced a methylurea group. **(B)** Manual docking of the antagonist used in this work, BIBO3304. The Y_1R inhibitor BIBO3304 is shown in red.

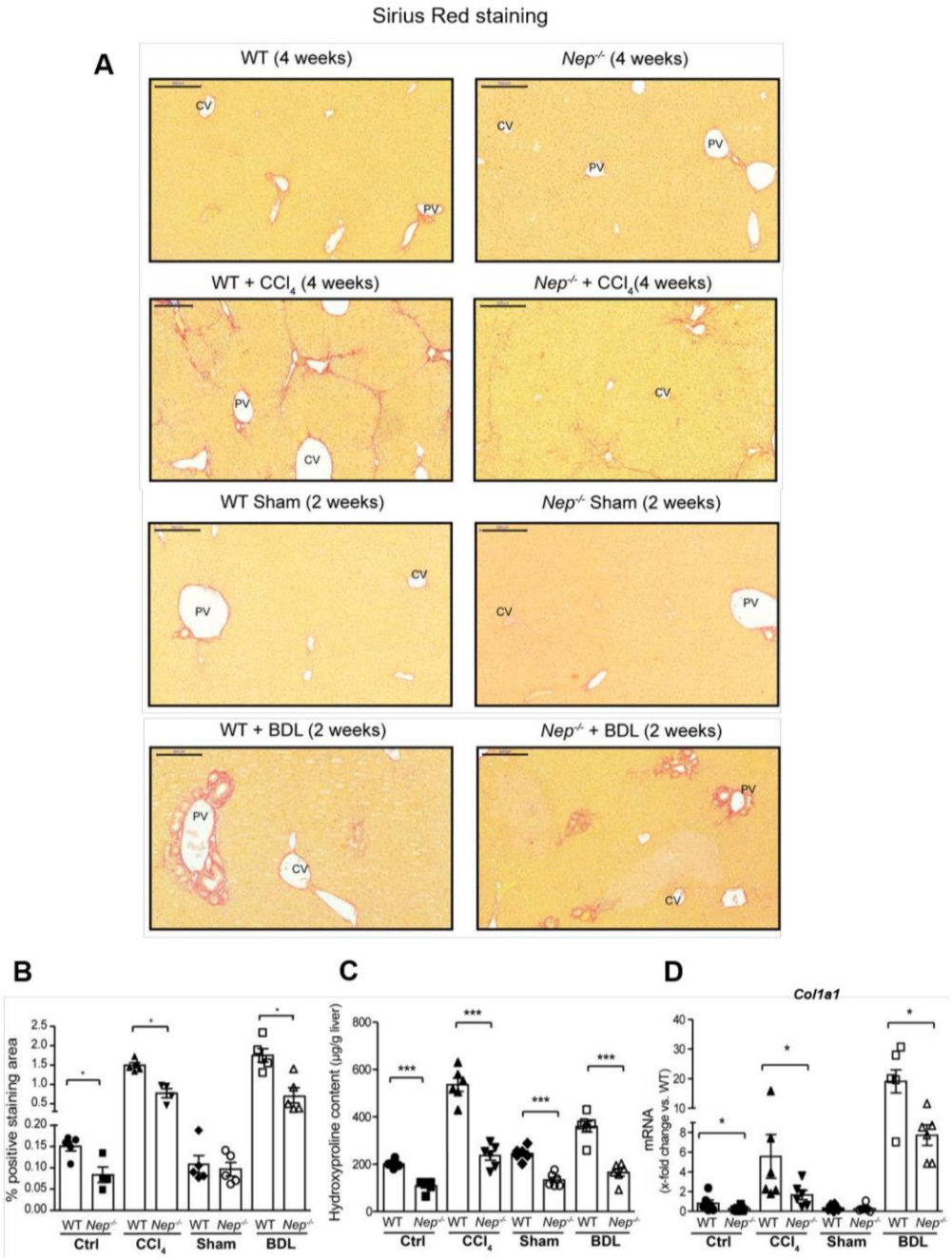

Supplementary Figure 8. *Nep* deletion reduces fibrosis in BDL- and CCl_4-treated mice. **(A-B)** Liver sections stained with Sirius red with their respective morphometric analysis. Central vein (CV) and portal vein (PV). Scale bar: 200 μm. **(C)** Hepatic hydroxyproline content and **(D)** hepatic *Col1a1* mRNA levels in BDL- and CCl_4-treated *Nep*$^{-/-}$ mice compared to WT mice, n=5/group. All data were normalized to the expression of *18S* RNA.

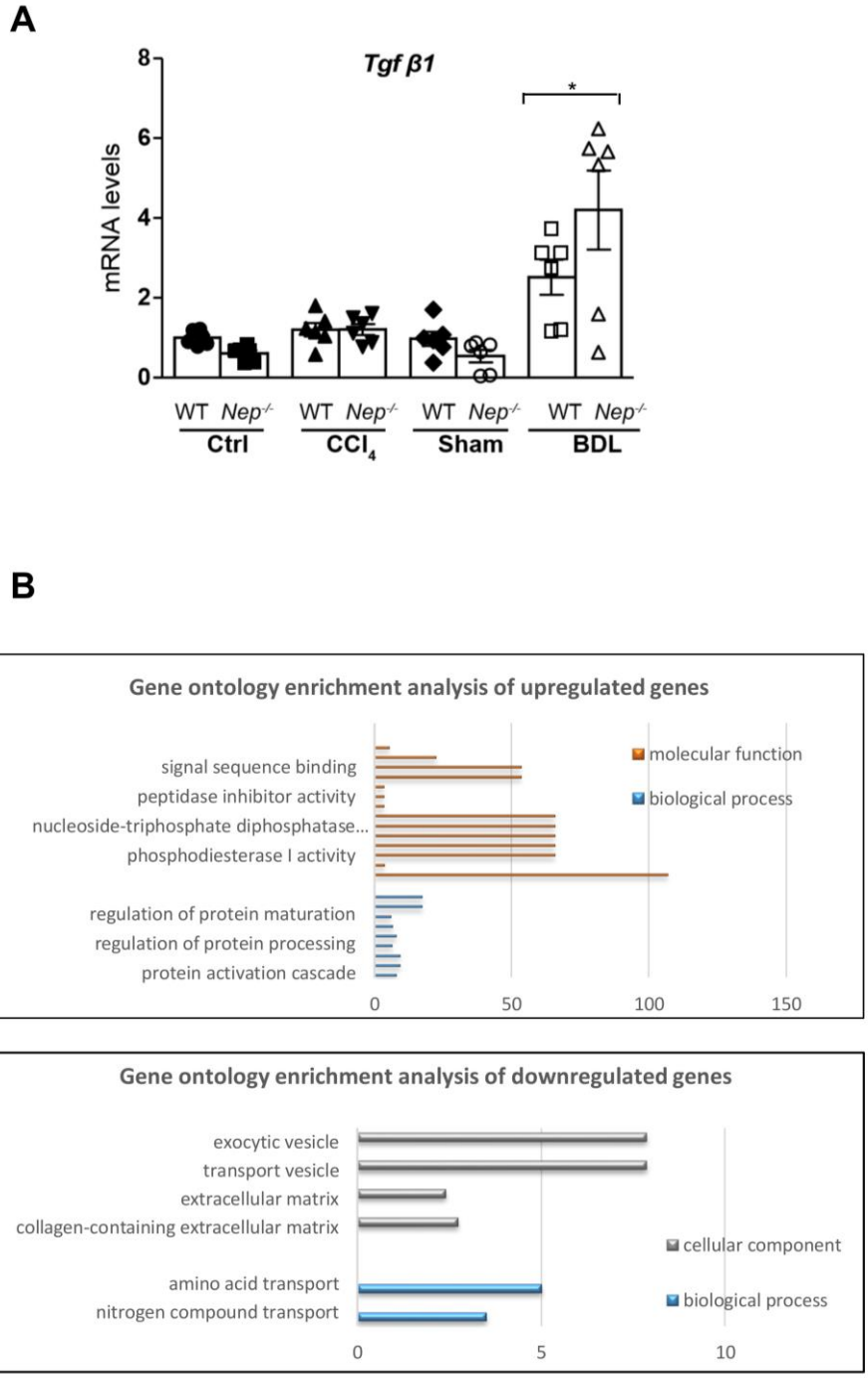

Supplementary Figure 9. BDL-treated *Nep*$^{-/-}$ mice show increased expression of *Tgfβ1*. **(A)** *Tgfβ1* mRNA expression in WT and CCl_4- and BDL-treated *Nep*$^{-/-}$ mice. BDL-*Nep*$^{-/-}$-treated mice showed increased expression of *Tgfβ1* compared to untreated mice, WT as well as *Nep*$^{-/-}$. All data were normalized to the expression of *18sRNA*. Results are expressed as mean ± standard error of the mean (SEM); n=6/group. *p<0.05 for BDL-treated *Nep*$^{-/-}$ mice compared to WT mice. **(B)** Gene Ontology analysis show the biological processes up/down regulated when hepatic NEP is highly or down expressed.

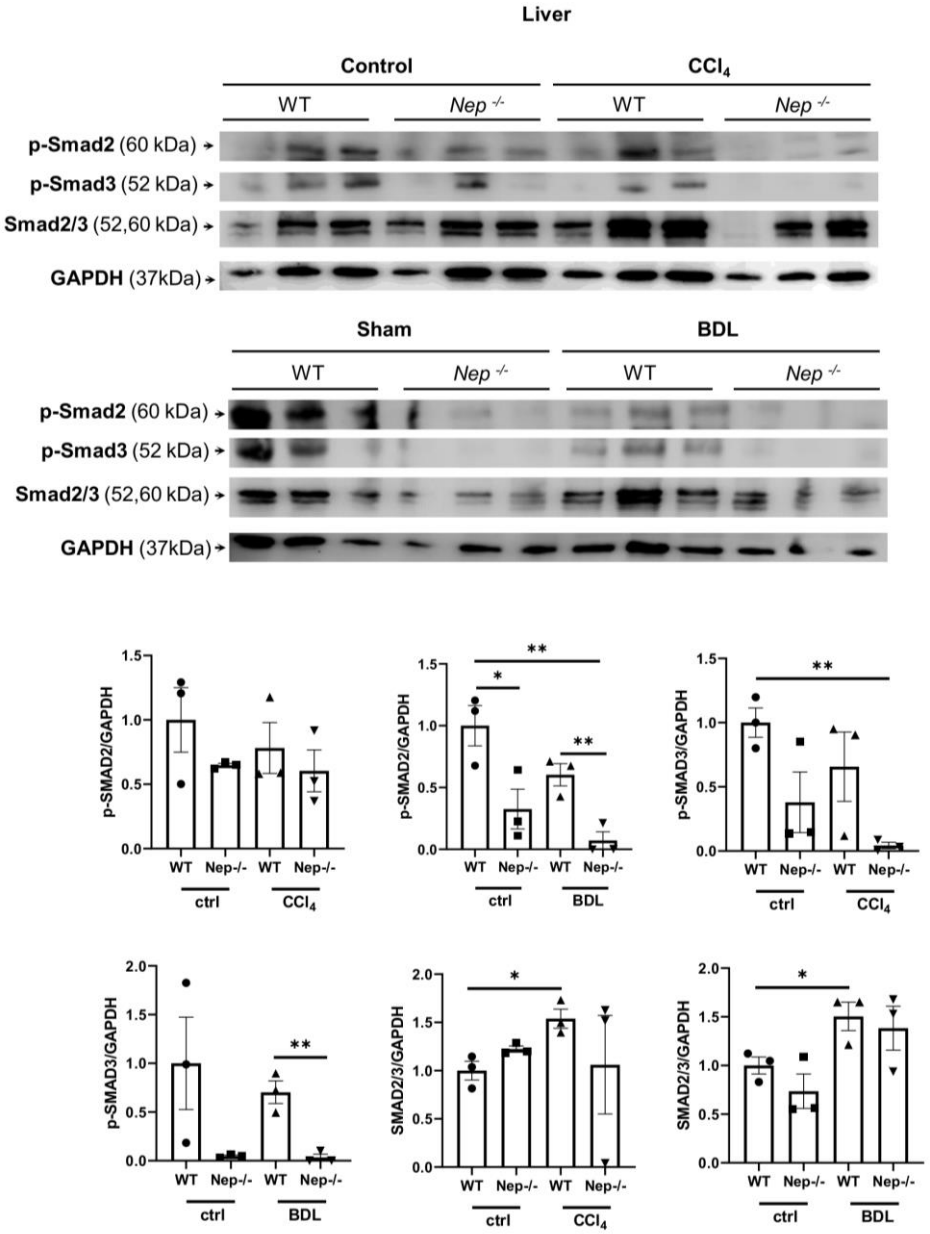

Supplementary Figure 10. Downstream effectors of Tgfβ1 pathway are decreased in *Nep*$^{-/-}$ mice. (A) Western blot analysis of mice livers comparing the expression of SMAD2/3 and their phosphorylated forms (pSMAD2/3) between WT mice and *Nep*$^{-/-}$ control vs. BDL and CCl_4. **(B)** Corresponding quantification of the signals compared to the loading controls GAPDH. Results are expressed as mean ± standard error of the mean (SEM); n=3/group. **p*<0.05 and ***p*<0.01.

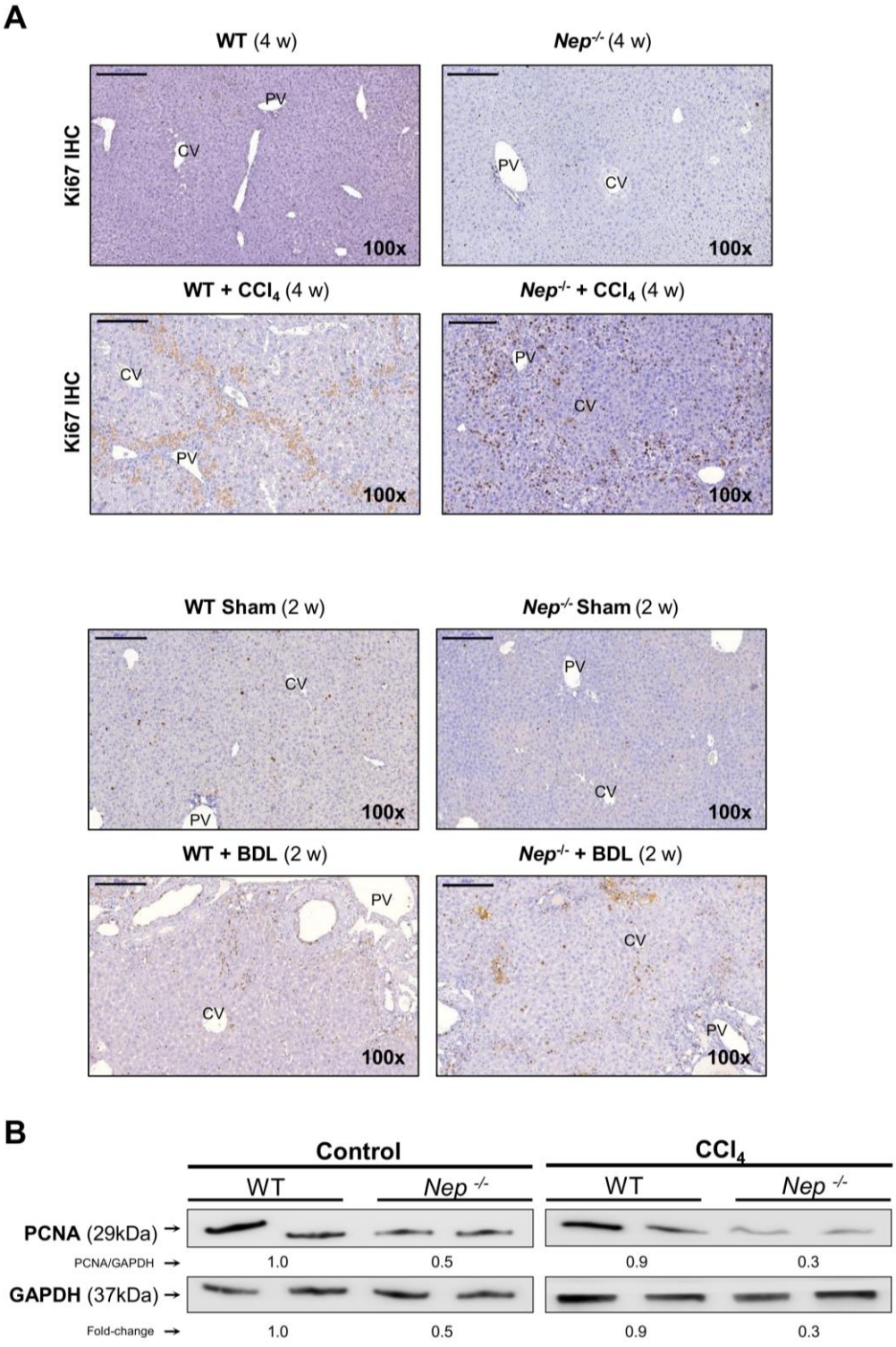

Supplementary Figure 11. NEP deletion does not change proliferation in livers from BDL- and CCl_4-treated *Nep*$^{-/-}$ mice compared to WT mice. (A) Ki67 IHC and **(B)** PCNA Western blot in CCl_4-treated WT compared to control *Nep*$^{-/-}$ mice**.** Values are expressed as fold-change *vs.* control WT mice. Scale bar=200μm.

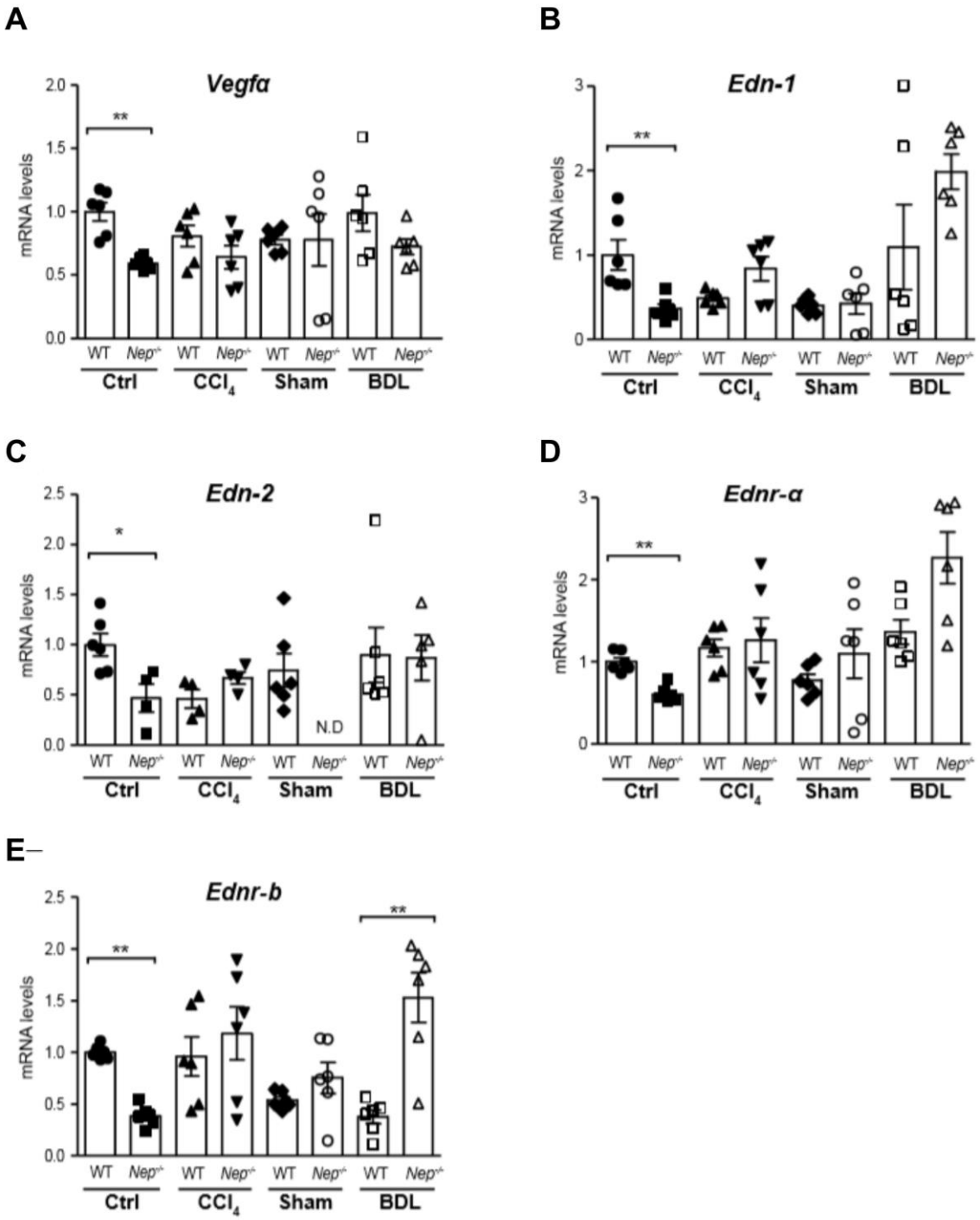

Supplementary Figure 12. BDL- and CCl_4-treated *Nep*$^{-/-}$ mice show no changes in *Vegfα*, *Edn-1*, *Edn-2*, *Ednra* and *Ednrb* mRNA expression compared to WT mice. (A) qPCR from liver lysates show unchanged *Vegfα* (vascular endothelial growth factor A) **(B)** *Edn1* (endothelin-1) **(C)** *Edn2* (endothelin-2) **(D)** *Ednra* (endothelin receptor type A) and **(E)** *Ednrb* (endothelin receptor type B) mRNA expression in BDL- and CCl_4-treated *Nep*$^{-/-}$ mice compared to WT mice. All data were normalized to the expression of *18s*RNA. Results are expressed as mean ± standard error of the mean (SEM); n=6/group. **p*<0.05, ***p*<0.01 for control WT *vs.* *Nep*$^{-/-}$ mice and for BDL-treated WT *vs.* *Nep*$^{-/-}$ mice.

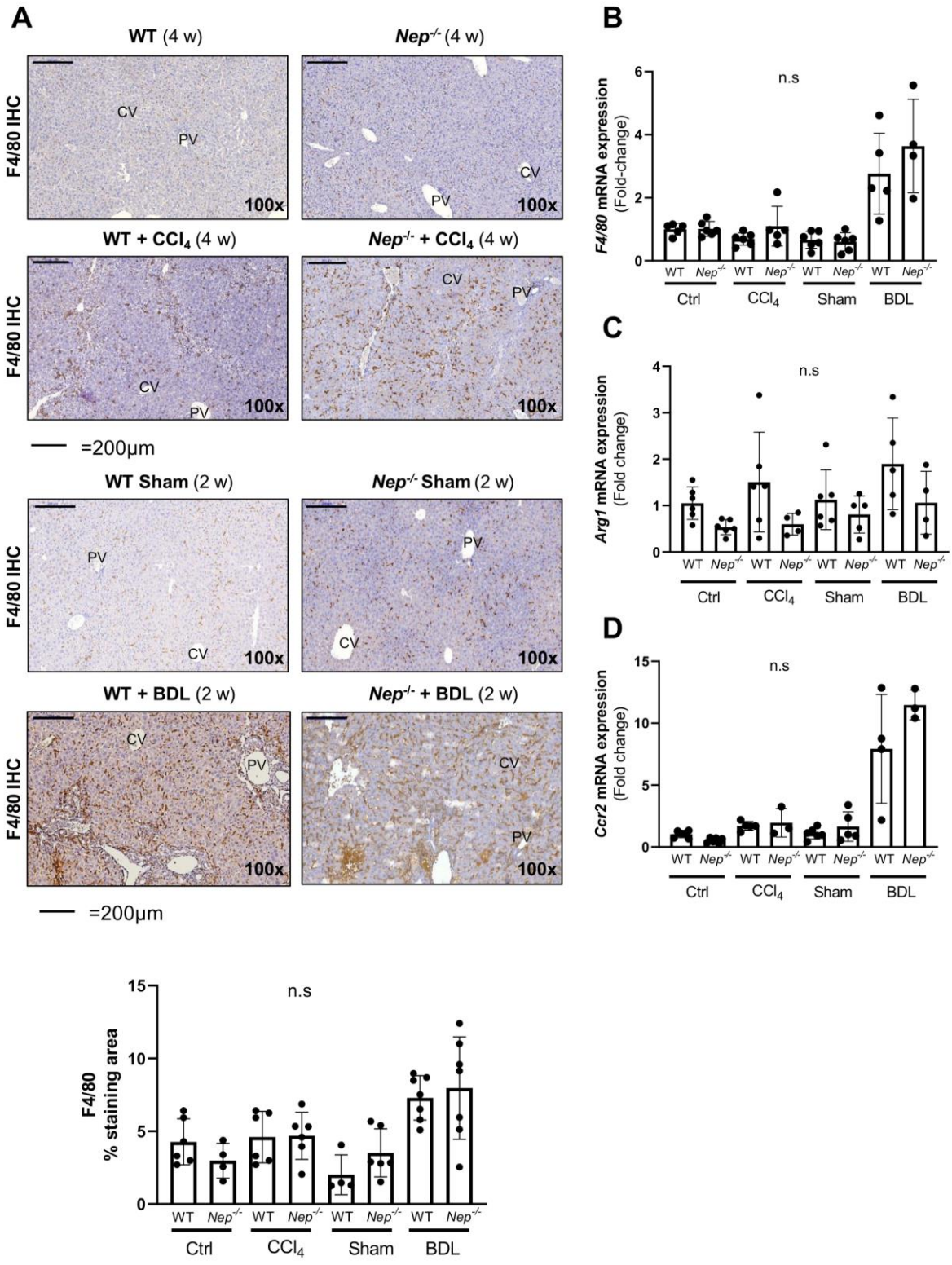

Supplementary Figure 13. Macrophage infiltration in WT *vs*. *Nep*$^{-/-}$ livers show no significant expression. Immunohistochemistry staining of F4/80 and quantification show no significant differences between the different treatments and/or WT *vs*. *Nep*$^{-/-}$ mice. qPCR from liver lysates show unchanged expression of F4/80, *Arg1* (arginase 1) and *Ccr2* (chemokine receptor 2). All data were normalized to the expression of *18s*RNA. Results are expressed as mean ± standard error of the mean (SEM); n=4-5/group. n.s. (not significant).

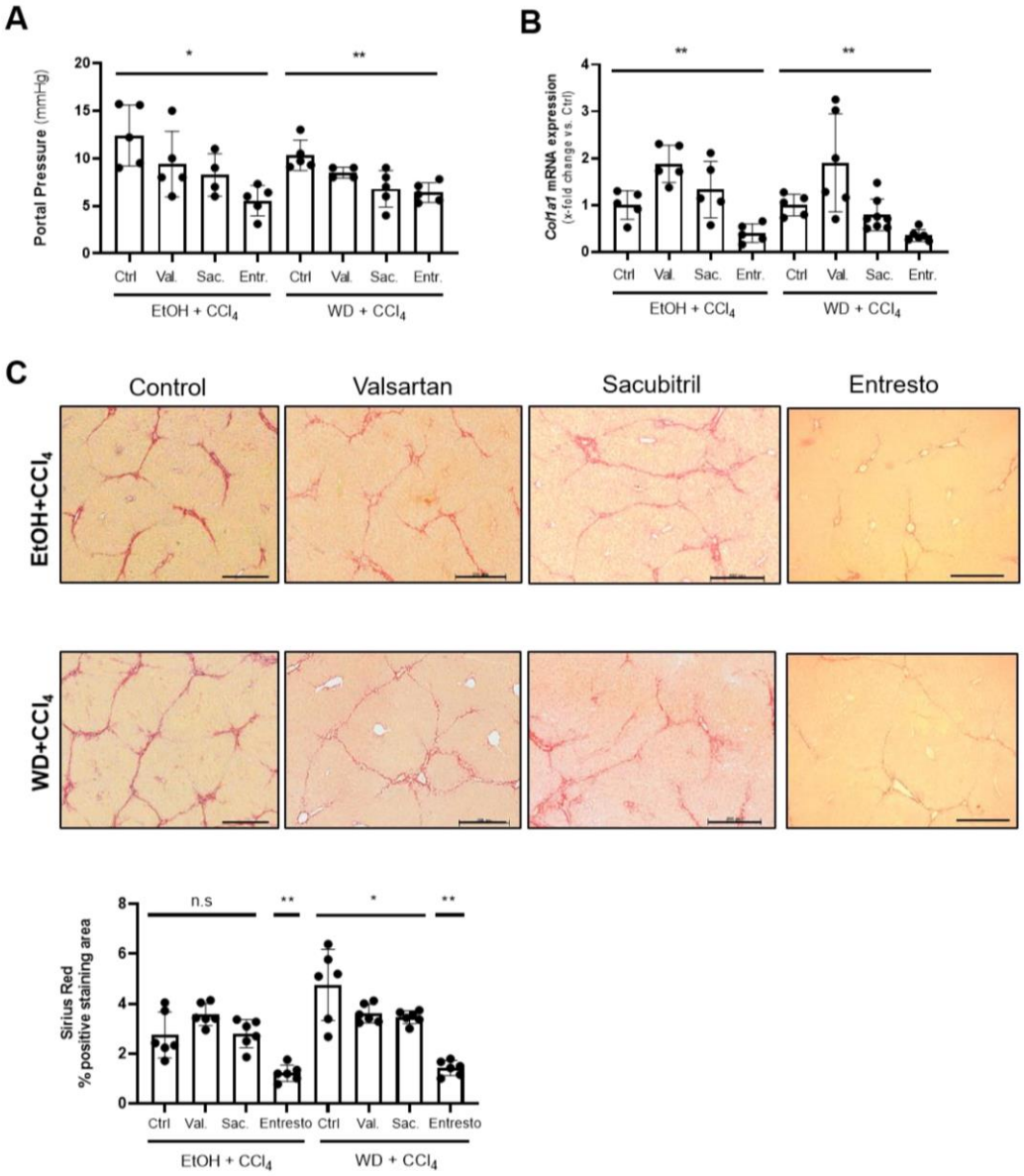

Supplementary Figure 14. Effect of valsartan and sacubitril in the progression of liver fibrosis. (A) Portal pressure measurements of the different mice treated with either valsartan, sacubitril and entresto compared to control mice. **(B)** *Col1a1* mRNA expression from the mice livers treated with the different drugs. All data were normalized to the expression of *18s*RNA. **p*<0.05, ***p*<0.01 for control mice *vs.*valsartan, sacubitril and Entresto mice.**(C)** Sirius red stainings and quantification of the mice groups treated with valsartan, sacubitril and Entresto.